Dynamics of Rubber Band Stretch Ejection

Xiang Li (lixiang@xauat.edu.cn)
Xi'an University of Architecture and Technology https://orcid.org/0000-0001-5932-1261
Bohua Sun
Xi'an University of Architecture and Technology https://orcid.org/0000-0002-0002-485X
Yi Zhang
Xi'an University of Architecture and Technology
yuanfan Dai
Xi'an University of Architecture and Technology

Research Article

Keywords: rubber band, elastodynamics, bending effect, hyperelastic materials, Maple

Posted Date: June 3rd, 2021

DOI: https://doi.org/10.21203/rs.3.rs-517306/v1

Nonlinear Dynamics manuscript

Dynamics of rubber band stretch ejection

Xiang Li · Bohua Sun · Yi Zhang · Yuanfan Dai

Abstract Why do stretched rubber bands not hit the hand after ejection? What is the mechanism behind the rubber band ejection dynamics? These questions represent a fascinating scientific problem. Because the size of a rubber band in the circumferential direction is much larger than that in the other two directions of its cross section, we regard the rubber band as a slender beam and establish a mathematical model of the dynamics of the rubber band stretching and ejection. Furthermore, we obtain the dependence of the dynamic curvature of the rubber band on the arc length and time. We used the finite element software ABAQUS to simulate the dynamic process of rubber band stretching and ejection. The simulation results and dimensional analysis were performed to examine the effect of the bending elastic rebound velocity. The mathematical model and simulation results revealed that the relationship between the curvature and time at the end of the rubber band ($s = 0$) was as follows: $\kappa \sim t^{-1/2}$. This research has guiding significance for the design of rubber bands as elastic energy storage devices.

Keywords rubber band · elastodynamics · bending effect · hyperelastic materials · Maple

Xiang Li · Bohua Sun · Yi Zhang · Yuanfan Dai
School of Civil Engineering & Institute of Mechanics and Technology, Xi'an University of Architecture and Technology, Xi'an 710055, China.
Tel.: +86 150-01-102877
Fax: +86 150-01-102877
E-mail: sunbohua@yahoo.com

Xiang Li
E-mail: lixiang@xauat.edu.cn

Yi Zhang
E-mail: yiyini2@xauat.edu.cn

Yuanfan Dai
E-mail: dyf@xauat.edu.cn

1 Introduction

Stretching, ejection, and retraction of objects are ubiquitous, including the retraction of flat elastic belts [1], the release of catapults [2], rubber band catapults, large catapults in amusement parks, and the strings of some musical instruments. Rubber band ejection is a familiar and interesting experience. The rubber band is stretched and released, and the whole movement process very fast. It is difficult to observe the retracted deformation state of the rubber band during the ejection process. However, it is amazing that the ejection of the stretched rubber band rarely hits the finger. [3] performed an experimental and theoretical study of two self similar retractions during rubber band ejection and explained the reason that the rubber band does not hit the hand. At the beginning of the stretching and ejection process, elastic retraction of the rubber band occurs. After the retraction to the initial state without strain, the rubber band as a whole moves forward at a uniform speed due to inertia. The finger can move out of the path of the rubber band during rebound so that it does not get hit by the rubber band. However, the dynamics are complicated.

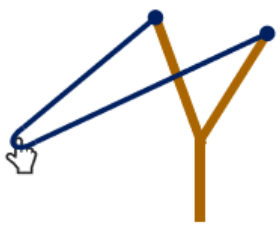

Fig. 1 Slingshot ejection model.

In the study of elastic retraction due to tension after release, the traditional unidirectional springback model

only considers the effect of tension and inertia ([4,5]), but the bending moment is very important in regions with high rates of bending ([6,7]) . When the front end of the rubber band begins to move, it bends dynamically in a manner similar to that of a straight beam or bar ([8,9]). [10] performed a detailed experimental study of the free contraction that occurs when one end of a stretched rubber band is released. [1] studied the dynamic instability of the elastic retraction by tension after release for flat rubber bands. The results of the study confirmed the existence and importance of longitudinal stress waves in the process of the tensile retraction of elastomers. ([11,12]) studied the dynamic response after the sudden release of stretched hyperelastic strings. Finite element simulation of this paper and the experimental results of [3], showed that in the process of the rubber band ejection and retraction, rubber bands are under tensile strain ϵ. The corresponding half angle of the wedge angle is ϕ, the initial length is ℓ_0 and the initial length after stretching is $(\epsilon+1)\ell_0$. When the rubber band is released at $t=0$, the back end of the rubber band will form an increasing bending area, and the speed of the reference point is V. [3] showed through experiments and theoretical analysis that when the influence of the bending effect is ignored in the process of elastic band pop-back shrinkage, the following elastic band springback speed relation is obtained: $\frac{V}{C}=\left(\frac{\epsilon}{\epsilon+1}\right)\left(\frac{1}{1-\sin\phi}\right)$.

The process of rubber band stretching and ejection is very complex, and it is meaningful to analyze the dynamic process. Thus, Section 2 of this paper begins with a mathematical model of the dynamics of rubber band stretching and ejection, and the dynamic process is comprehensively analyzed. In Section 3, the finite element software ABAQUS is used to verify the experimental results of [3] to ensure that the simulation results and data are correct and to verify the relationship between the curvature in the mathematical model and the arc length and time. Based on the results of dimensional analysis, simulations of the stretched ejection of rubber bands with different thicknesses were conducted considering the influence of the effect of bending. Section 4 draws conclusions.

2 Mathematical model of stretched rubber band ejection dynamics

During the springback process of rubber bands, a bent region with increasing size will form at the back, as shown in Fig. 2.

[3] used a beam model to study the self-similar retraction behavior during rubber band ejection. Here, we

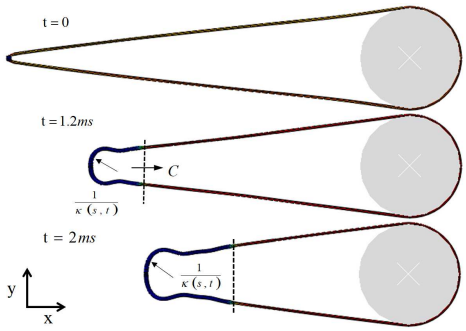

Fig. 2 Rubber band stretching and ejection diagram

model the region after the longitudinal wave passes as an constant-length beam based on the Euler–Bernoulli beam theory ([13,14,15]). The beam cross-sectional area is A, the cross-sectional moment of inertia is I (rectangular section $I=\frac{1}{12}bh^3$, b is the width, h is the thickness, $I=\frac{1}{4}\pi r^4$, and r is the radius). The following relationships are defined: $\frac{\partial x}{\partial s}=\cos\theta(s,t)$, $\frac{\partial y}{\partial s}=\sin\theta(s,t)$, where $\theta(s,t)$ is the angle between the tangent and the x-axis. The small deflection vibration equation of the beam [6] is as follows:

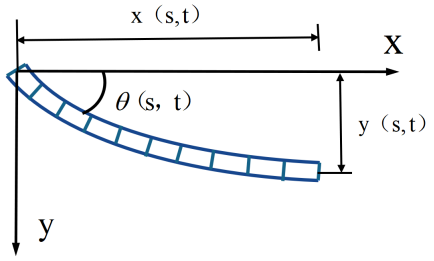

Fig. 3 Beam theory mathematical model of stretched rubber band rebound

$$EI\frac{\partial^4 y}{\partial s^4}+\rho A\frac{\partial^2 y}{\partial t^2}=0, \tag{1}$$

where $y(s,t)$ is the deflection, s is the arc length, and t is time.

The beam theory model contains the rotation angle $\theta=\frac{\partial y}{\partial s}$ and the curvature $\kappa=\frac{\partial^2 y}{\partial s^2}$. Under the assumption of a small displacement [6], to facilitate the study of the elastic band springback process in this paper, Eq.1 is expressed in the form of a rotation angle $\theta(s,t)$ as follows:

$$EI\frac{\partial^4 \theta}{\partial s^4}+\rho A\frac{\partial^2 \theta}{\partial t^2}=0, \tag{2}$$

Its self-similar solution is

$$\begin{aligned}\theta(s,t) =& C_1 \frac{s^2}{t}\ \text{hypergeom}\left(\left[\frac{1}{2},1\right],\left[\frac{3}{4},\frac{5}{4},\frac{3}{2}\right],-\frac{\rho A s^4}{64EIt^2}\right)\\ &+ C_2\ \text{Fresnels}\left(\frac{1}{\sqrt{2\pi}}\left(\frac{\rho A}{EI}\right)^{\frac{1}{4}}\frac{s}{\sqrt{t}}\right)+\\ &C_3\ \text{FresnelC}\left(\frac{1}{\sqrt{2\pi}}\left(\frac{\rho A}{EI}\right)^{\frac{1}{4}}\frac{s}{\sqrt{t}}\right)+C_4,\end{aligned} \tag{3}$$

where C_1, C_2, C_3, and C_4 are unknown parameters. Applying the $\theta(s,t)$ boundary conditions: $\theta(0,t)=\frac{\pi}{2}$, $\theta(s,t\to 0)=\phi$, $\frac{\partial^2\theta}{\partial s^2}(0,t)=0$, and $\frac{\partial^3\theta}{\partial s^3}(0,t)=0$, we determine that $C_1 = C_2 = 0$, $C_3 = (2\phi-\pi)$, and $C_4=\frac{\pi}{2}$. Thus,

$$\theta(s,t)=\frac{\pi}{2}+(2\phi-\pi)\ \text{FresnelC}\left(\frac{1}{\sqrt{2\pi}}\left(\frac{\rho A}{EI}\right)^{\frac{1}{4}}\frac{s}{\sqrt{t}}\right). \tag{4}$$

The material parameters of the rubber band were selected as follows: the radius of the circular section r = 0.8 mm, the diameter of the rubber band D = 64 mm, the density $\rho = 1.3\ g\cdot cm^{-3}$, E = 1.1 MPa, and the initial wedge half-angle $\phi = 11.6°$.

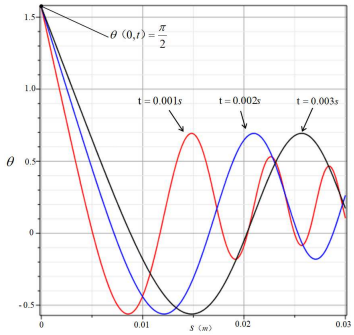

Fig. 4 Variation of θ with s. The curves shown in red, blue, and black correspond to times t = 0.001, 0.002, and 0.003 s.

Fig. 4 - Fig. 6 show the following. (1) When the arc length s is zero, $\theta=\frac{\pi}{2}$. (2) θ increases with the arc length s during the ejection of the rubber band. It then gradually decreases to zero and then continues to increase in the opposite direction, showing periodic changes. With the increase in the arc length s, θ changes more drastically. (3) During the rebound of the stretched rubber band in a small arc range, the angle changes smoothly with time. (4) In a short time period after the rubber band is released, the angle changes

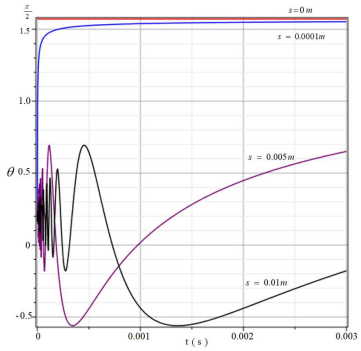

Fig. 5 Variation of θ with t. The arc lengths of the curves shown in red, blue, purple, and black correspond to s = 0, 0.0001, 0.005, and 0.01 m.

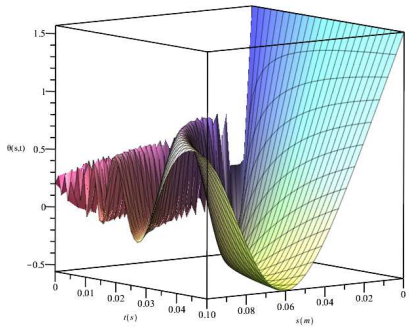

Fig. 6 Three-dimensional phase diagram of $\theta(s,t)$ as a function of time t and arc length s.

rapidly, and it finally increases and changes slowly with time.

We define a dimensionless quantity $\xi = s/\left[\left(EIt^2\right)/(\rho A)\right]^{1/4}$. Thus,

$$\theta(\xi)=\frac{\pi}{2}+(2\phi-\pi)\text{FresnelC}\left[\frac{\xi}{\sqrt{2\pi}}\right]. \tag{5}$$

According to Eq.4 and Eq.5, we can define the complementary angle of $\theta(s,t)$ as $\varphi(\xi)$, that is, $\varphi(\xi) = \pi/2-\theta(s,t)$. We then have the following: $\varphi(\xi) = (\pi - 2\phi)$ Fresne1C $\left(\frac{\xi}{\sqrt{2\pi}}\right)$. This differential equation is the same as that obtained by [3] when modeling two self-similar retractions of a tensile elastic wedge. $\varphi(\xi)$ is obtained by taking the first derivative of ξ, as follows: $\varphi'(\xi) = \frac{(\pi-2\phi)\cos\left(\frac{\xi^2}{4}\right)}{\sqrt{\pi}}$. When $\varphi'(\xi)=0$ and $\varphi(\xi)$ has extreme values, $\xi=\sqrt{2(2n+1)\pi}$, $\quad n=0,1,2...$

The analysis showed that when $\xi=\sqrt{2\pi}$, the complimentary angle $\varphi(\xi)$ had a maximum value, at which time the rubber band stretched and retracted to the initial state without strain. As the variable ξ increased gradually, the degree of change in the angle of rotation

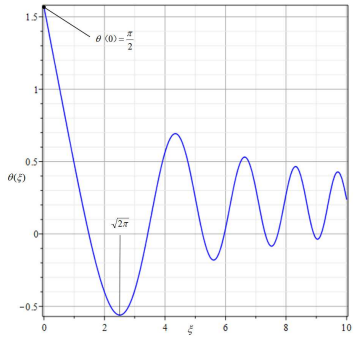

Fig. 7 Variation of $\theta(\xi)$ with ξ.

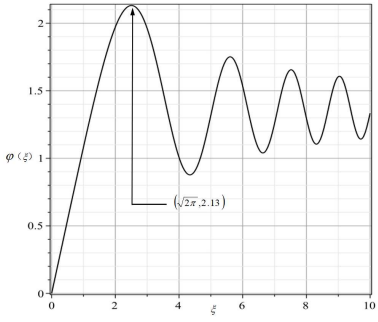

Fig. 8 Variation of $\varphi(\xi)$ with ξ.

tended to be gentle. Before the maximum supplementary angle appeared, the recovery process of the elastic energy of the rubber band occurred, after which the rubber band moved in the ejection direction overall.

Combined with Euler–Bernoulli beam theory [14], the curvature κ in the process of stretching and springback of rubber band is obtained by Eq.4 as follows:

$$\kappa(s,t) = \frac{\partial\theta_{(s,t)}}{\partial s} = \frac{(2\phi-\pi)}{\sqrt{2\pi}}\left(\frac{\rho A}{EI}\right)^{\frac{1}{4}} t^{\frac{1}{2}} \cos\left[\frac{1}{4}\left(\frac{\rho A}{EI}\right)^{\frac{1}{2}}\frac{s^2}{t}\right]. \quad (6)$$

When the dimensionless quantity $\xi = s/\left[(EIt^2)/(\rho A)\right]^{1/4}$ and the complementary angle $\varphi(\xi)$ takes the maximum value, $\xi = \sqrt{2\pi}$. Substituting this result into Eq.6 , $\kappa = 0$ when the supplementary angle has the maximum value during the rebound of the rubber band, i.e., the curvature is zero. At this time, there is no bending moment, and the rubber band elastically retracts to its unstretched initial state.

At the origin, where $s = 0$, we have the following:

$$\kappa = \frac{(2\phi-\pi)}{\sqrt{2\pi}}\left(\frac{\rho A}{EI}\right)^{\frac{1}{4}} t^{-\frac{1}{2}}. \quad (7)$$

Fig. 9 -Fig. 11 show the following: (1) the curvature changes more sharply with the increase in the arc length, and the fluctuation range of the curvature decreases with the increase in time when the arc length is

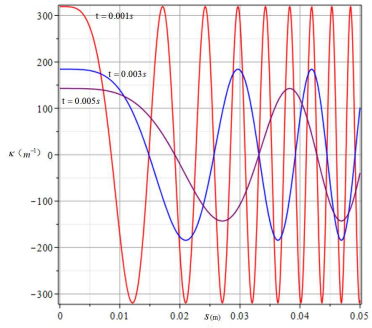

Fig. 9 Variation of curvature κ with arc length s (curvature is positive). The curves shown in red, blue, and purple correspond to times $t = 0.001$, 0.003, and 0.005 s.

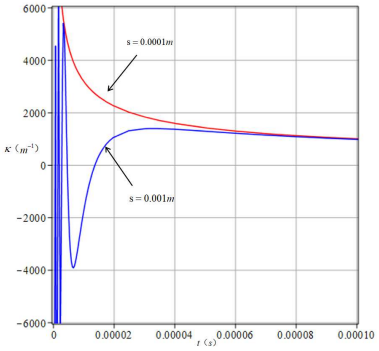

Fig. 10 Variation of κ with time t (curvature is positive). Curves shown in red and blue correspond to arc lengths of $s = 0.0001$ and 0.001 m.

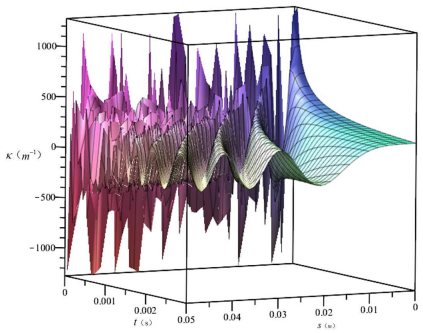

Fig. 11 Phase diagram of curvature $\kappa(s,t)$ as a function of time t and arc length s (curvature is positive).

constant; (2) within a small range of time t after release, the curvature changes dramatically during the springback process and tends to be flat as time increases; (3) there is a non-zero curvature at the origin (s=0), that is, there is an initial curvature at the origin and the curvature is the maximum curvature; with the increase in time, the curvature at the origin gradually becomes smaller and finally decreases to zero, which is also consistent with the phenomenon observed in the simulation.

The differential equation for the deflection of the beam during the rebound process after rubber band

ejection can be obtained. The moment in the beam is $M = -EI\frac{\partial\theta}{\partial s}$, which is expressed as follows:

$$M(s,t) = \frac{\pi - 2\phi}{\sqrt{2\pi}}(\rho A)^{\frac{1}{4}}(EI)^{\frac{3}{4}}t^{-\frac{1}{2}}\cos\left[\frac{1}{4}\left(\frac{\rho A}{EI}\right)^{\frac{1}{2}}\frac{s^2}{t}\right]. \tag{8}$$

According to Eq.6 and Eq.8, the curvature and bending moment of the bending region have the same relationship with the arc length and time. There is only one constant difference between the expressions of the curvature and bending moment, and this constant depends on the cross section geometry and material parameters. Similarly, there is an initial bending moment at the origin, and the bending moment changes sharply with the increase in the arc length s. In a short period of time after the rubber band is released, the bending moment changes very sharply, and the change tends to be gentle with the increase in time.

The shear force in beam is $Q = -\frac{\partial M(s,t)}{\partial s}$. Thus,

$$Q(s,t) = \frac{2\phi - \pi}{2\sqrt{2\pi}}(\rho A)^{\frac{3}{4}}(EI)^{\frac{1}{4}}st^{-\frac{3}{2}}\sin\left[\frac{1}{4}\left(\frac{\rho A}{EI}\right)^{\frac{1}{2}}\frac{s^2}{t}\right]. \tag{9}$$

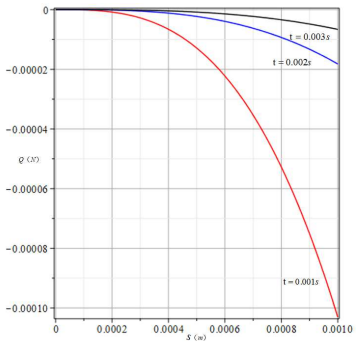

Fig. 12 Variation of shear force Q with arc length s. The curves shown in red, blue, and black correspond to times t = 0.001, 0.002, and 0.003 s.

Fig. 12-Fig. 14 show that (1) the shear force Q is zero at the origin, which satisfies a symmetry condition during elastic ejection, (2) the shear force Q increases gradually with the arc length s, and it increases faster and faster, and (3) the shear force changes sharply over a short time, whereas the arc length shear force decreases gradually to zero with time.

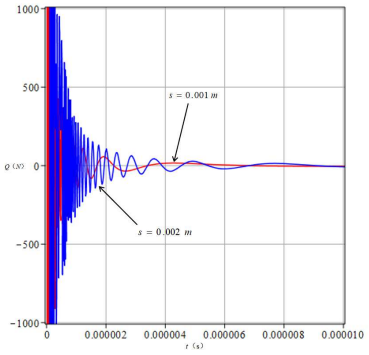

Fig. 13 Variation of shear force Q with time t. Curves shown in red and blue correspond to arc lengths of s = 0.001 and 0.002 m.

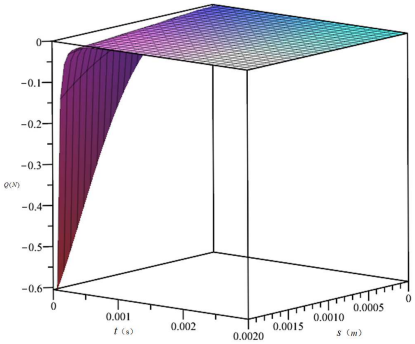

Fig. 14 Three-dimensional phase diagram of shear force Q as a function of arc length s and time t.

3 Finite element simulation of rubber band stretching ejection dynamics

We used the material and size of the rubber band used by [3] to verify the experimental and theoretical results and to ensure the feasibility of the finite element model and the accuracy of the extracted data.

3.1 Extraction of experimental parameters of superelastic materials

In this paper, the experimental data, the stress–strain curve of the rubber band material Fig. 15, and the material parameters reported by [3] were used in the simulation (Table 1).

A rubber band is a hyperelastic material ([16,17,18]) . Based on the assumption that isotropy and volume are approximately incompressible, a variable-density function is usually used to characterize rubber. At present, the polynomial strain energy function ([19,20,21]) (generalized Mooney–Revlin function), which is widely used in finite element analysis, is expressed as follows: $U = \sum_{i+j=N}^{N} C_{ij}\left(I_1 - 3\right)^i\left(I_2 - 3\right)^j + \sum_{k=1}^{N}\frac{1}{d_k}\left(\sqrt{I_3} - 1\right)^{2k}$, where N is the order of the function, C_{ij} and d_k are

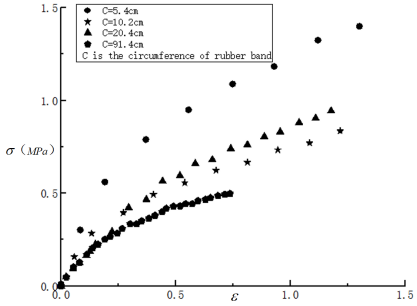

Fig. 15 Stress–strain curves of various kinds of rubber bands. The constitutive parameters of the rubber bands were obtained from the report of [3] on rubber band ejection.

material constants, which are usually obtained by experiments, and I_1, I_2, and I_3 are strain invariants of order 1, 2, and 3, respectively.

The finite element software ABAQUS was used to analyze the experimental material data, and the two-parameter Mooney–Revlin model ([22,23]) , $W = C_{10}\,(I_1 - 3) + C_{01}\,(I_2 - 3)$, was used to study the elastic band material, as shown in Fig.15, because it has better stability.

Table 1 Rubber band material parameters

quantities	units	I	II	III	IV
circumference	C(cm)	5.4	10.2	20.4	91.4
width	b(mm)	1.2	13	1.6	25.4
thickness	h(mm)	1.1	1.7	2.0	1.7
density	$\rho\,(\mathrm{gcm}^{-3})$	0.8	1.2	1.3	1.1
elastic modulus	E(MPa)	1.5	1.1	1.1	1.1
coefficient	C_{10}	0.069	0.203	0.187	-0.024
coefficient	C_{01}	0.586	0.046	0.122	0.34

Table.1. Dimensions and material parameters of rubber bands with rectangular cross sections were obtained from the report of [3] on rubber band ejection. A circular cross section of the rubber band was assumed, and the parameters were as follows: $r = 0.8$ mm, $D = 64$ mm , $\rho = 1.3\ g \cdot cm^{-3}$, $E = 1.1$ MPa, $\phi = 11.6°$, $C_{10} = 0.187$, and $C_{01} = 0.122$.

3.2 Simulation results and verification

The material parameters for the selected model were as follows: $C = 20.4$ cm, b =1.6 mm, h =1.9 mm, $\rho = 1.3\ g \cdot cm^{-3}$, $E = 1.1$ MPa, $\epsilon = 0.476$, $\phi = 14°$, $C_{10} = 0.187$, and $C_{01} = 0.122$. Rigid cylindrical contact was specified at the front end of the stretched rubber band, the normal and tangential directions were both hard contacts, and the rubber band was modeled using the solid C3D8R units of the ABAQUS software. The finite element model results for the stretching and ejection of the rubber band with the above material parameters are shown in Fig.16 (see the attachment for the simulation dynamics results).

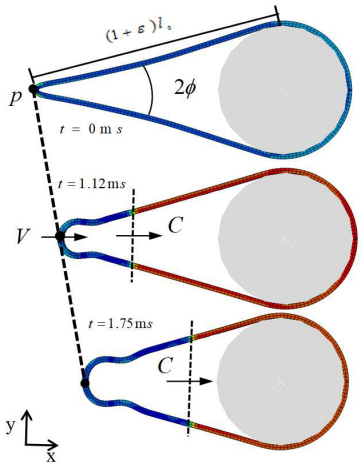

Fig. 16 Stretched rubber band ejection simulation.

Using the finite element model established above, the midpoint p of the end of the rubber band (Fig. 16) was taken as the reference point, and its speed was V.

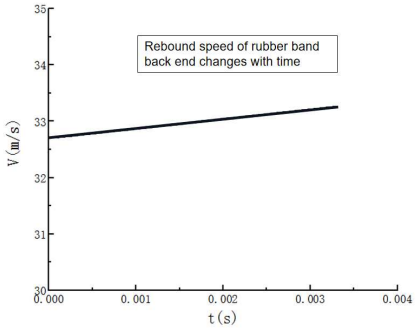

Fig. 17 Rear rebound speed of the rubber band, V

The rebound speed V (Fig. 17) at the back end of rubber band increased with time, but the overall change was small. In fact, after the release of the stretched rubber band, the rubber band began to shrink, and the rear end moved in the ejection direction, which indicated that the elastic recovery of the stretched rubber band was accompanied by the rapid release of elastic energy.

After the elastic recovery process of the rubber band was complete, the whole rubber band moved in the ejection direction due to inertia. According to Newton's second law, $F = ma$, when the external force is F=0, the speed of the elastic rebound point is uniform along the ejection direction.

Using the same modeling method, combined with the experimental theory of [3], the stretching and ejection of elastic bands with different strain rates, wedge half angles, materials, and sizes were simulated (the results are shown in Fig. 18).

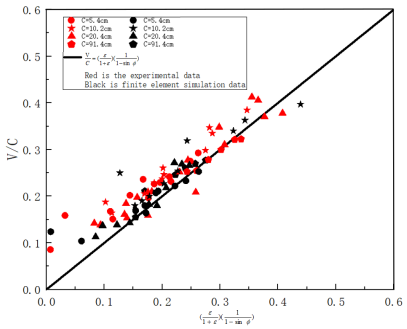

Fig. 18 Experimental results of [3] and the results of the finite element simulation in this paper (rectangular cross sections).

In Fig. 18, the red points are the experimental data of [3], and the black points are the simulation results of this work. The results were consistent with each other, and the difference between them was small, indicating the accuracy of the simulation and extracted data in this work. The theoretical results obtained by [3] ignored the bending effect, and these results were different than the simulation results in this paper, indicating that the influence of the bending effect on this dynamic process must be further discussed.

Based on the elastic stretching dynamics model of the ejection process, we examined the motion of the elastic rebound endpoint ($s = 0$). The curvature is expressed as follows: $\kappa = \frac{2\phi-\pi}{\sqrt{2\pi}} \left(\frac{\rho A}{EI}\right)^{\frac{1}{4}} t^{-\frac{1}{2}}$.

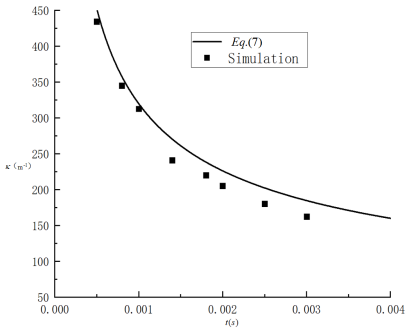

Fig. 19 Variation of curvature κ with time t at the end of the elastic during retraction (curvature is positive).

Fig. 19 shows the simulation results of this paper (the model parameters are shown in Table. 1. The solid line represents the theoretical results obtained by introducing the beam mathematical model. The curvature of the end of the rubber band during the retraction process decreased with time and finally reached zero, with a decreasing trend of $\kappa \sim t^{-\frac{1}{2}}$. This agrees with the theoretical relationship given by Eq. 7 and verifies the accuracy of the mathematical model of the stretched rubber band ejection dynamics.

3.3 Influence of bending effect on tensile ejection dynamics

Through dimensional analysis (see the appendix), we determine the equation for the speed of the rebound process: $\frac{v}{c} = f(\epsilon, \phi, \frac{h}{b})$.

In the simulation process, we can directly see the change of the bending area in the springback process of the rubber band. We selected the simulation results of the model shown in Fig. 16, where $\epsilon = 0.476$ and $\phi = 14°$. We ignored the influence of bending effect (Fig. 20).

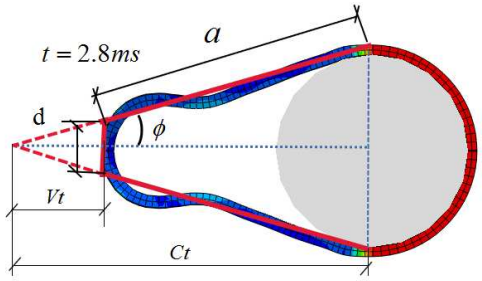

Fig. 20 During the rebound process of the rubber band, the influence of the bending effect is ignored

When the longitudinal wave reaches the cylinder, the position of the longitudinal wave is $ct = (1+\epsilon)\ell_0 \cos\phi$, and the sum of half the length of the upper side and one leg of the trapezoid was approximately equal to ℓ_0, that is, $\ell_0 = d/2 + a$. a and d are the lengths of trapezoid leg and the upper and lower sides, respectively. The geometric relationship $ct\tan\phi - a\sin\phi = d/2$ yields the following: $a = \frac{1-(1+\varepsilon)\sin\phi}{1-\sin\phi} l_0$, $d = \frac{2\varepsilon\, l_0\, \phi}{1-\sin\phi}$. The geometric relationship is $\frac{V}{C} = \frac{d}{2}/(ct \cdot \tan\phi)$. Therefore, $\frac{V}{C} = \left(\frac{\epsilon}{1+\epsilon}\right)\left(\frac{1}{1-\sin\phi}\right)$. According to this equation, the dynamics equation obtained by ignoring the influence of the bending effect on the springback dynamics of the rubber band (which is independent of the cross-sectional shape of rubber band at this time) is consistent with the result of [3]. At the same time, it was proven that the dimensional analysis of the elastic rebound dynamics was correct.

Considering the influence of the bending effect on the dynamics of the whole retraction process, the dynamic relationship between the velocity V and the longitudinal wave velocity C is as follows: $\frac{V}{C} = f\left(\epsilon, \phi, \frac{h}{b}\right)$. To ensure that the strain ϵ, wedge half angle ϕ, and rubber band width b are fixed values, rubber bands with different thicknesses h are used for the simulation, and the simulation results are shown in Fig. 21.

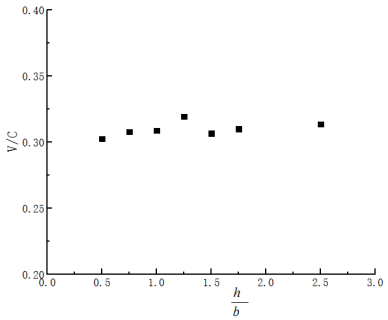

Fig. 21 Influence of thickness h on the springback dynamics

As shown in Fig. 21, during the springback process of rubber bands with different thicknesses h, the thickness of the rubber band has little influence on the springback dynamics. This is mainly because the thickness h is smaller than the diameter of the rubber band and the main stretching length scale, and the influence of the thickness h on the elastic dynamics is not significant. It is speculated that rubber bands with different cross-sectional shapes exhibit the same dynamics during stretching ejection when considering the bending term. The rubber band is stretched until the wedge half angle is ϕ and has strain ϵ. The tensile stress inside the rubber band is dominant when stretching and retracting, and the bending effect is small at this time. When the rubber band is retracted to a certain extent, the influence of the tensile stress inside the rubber band is significantly reduced, and the influence of bending gradually increases. Thus, the influence of the bending tensile ejection dynamics cannot be ignored.

Considering the influence of the bending of the rubber band during springback, the experimental results of [3] and the simulation results in this paper were fitted linearly, as shown in Fig. 22.

There was a significant difference between the two results. Therefore, considering the influence of the bending area on the ejection of the stretched rubber band, the coefficient α is introduced to modify the springback velocity relation as follows:

$$\frac{V}{C} = \alpha\left(\frac{\epsilon}{\epsilon+1}\right)\left(\frac{1}{1-\sin\phi}\right), \tag{10}$$

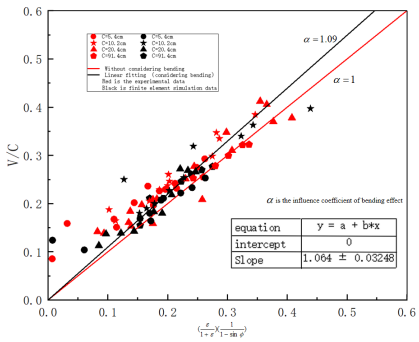

Fig. 22 Linear fit of experimental [3] and the simulation results in this paper (rectangular cross sections).

where α was determined by fitting to be 1.09.

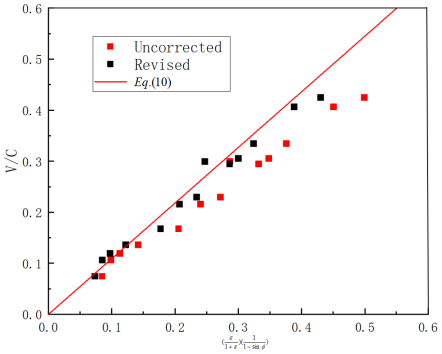

Fig. 23 Simulation results for circular sections with and without bending.

Based on a previous study, a circular cross section (Table. 1) was used to simulate the results (Fig. 23). The fitting degree of the theoretical and finite element simulation results were improved by considering the correction factor of the bending moment. When the cross-sectional dimensions of the rubber band were small compared with the main length scale, the influence of the cross-sectional shape and size on the elastomer stretching and ejection velocity can be ignored within a certain range of requirements.

4 Conclusions

The conclusions of this research are as follows:

(1) A simple Euler–Bernoulli beam model was used to analyze the stretched elastic band ejection process. The results showed that the simple beam model of the dynamics can describe the whole ejection process well.

(2) The bending area changed constantly during the rebound of the rubber band. According to the mathematical model of this paper, the curvature relationship is given by Eq.6. Combined with the finite element simulation results, the results at the origin were verified

and fit well with experimental data. In addition, the curvature value at the origin of the rubber band was the largest in the process of stretching and ejection, and it had an initial curvature that was not zero. The variation of the curvature at the origin with time t and arc length s is given by Eq.7.

(3) By solving and analyzing the mathematical model of the stretched rubber band ejection dynamics, we determined that the angle θ, curvature κ, bending moment M, and shear force Q change sharply in a short initial period during the ejection. This also agreed with the fact that a large amount of energy is released rapidly at the moment of ejection, resulting in significant spring-back deformation.

(4) The factors that affect the rebound velocity relationship $\frac{V}{C}$ in the process of stretching and ejection can be determined by dimensional analysis. The simulations presented in this paper were in good agreement with the experimental results of Oratis and Bird, which proved the accuracy of the simulation and data extraction. Without considering bending, the theoretical results of Oratis and Bird were consistent with the experimental and simulation results, but there were some differences. In this paper, the influence of the bending effect on the stretched elastic ejection was considered. By changing the cross-sectional thickness h, which affects the bending moment, and comparing the experimental results of Oratis and Bird and the simulation data in this paper, the correction coefficient of $\alpha = 1.09$ to account for bending effect was obtained.

Conflict of interest

The authors declare that they have no conflict of interest.

funding

This research did not receive any specific grant from funding agencies in the public, commercial, or not-for-profit sectors.

Availability of data and material

All data generated or analyzed in this study are included in this paper, and more detailed data can be obtained from the corresponding authors according to reasonable requirements.

Authors' contributions

Xiang Li conceived ,designed the study ,wrote the whole paper and coordinated all inputs. Bohua Sun provided input for the overall theme of the paper and participated in the revision of manuscript. Yi Zhang participated in the finite element simulation (especially Figure 9). Yuanfan Dai participated in the analysis of material parameters in finite element simulation (especially Figure 8). All authors gave final approval for publication and agree to be held accountable for the work performed there in.

My Appendix

Dimensional analysis of rubber band stretch ejection dynamics:

Based on dimensional analysis theory [24], seven parameters were determined (see the table below), among which there are three basic dimensions: L, M, and T.

Table 2 Dimensions of physical quantities

variable	symbol	dimension
width	b	L
thick	h	L
density	ρ	ML^{-3}
elastic Modulus	E	$ML^{-1}T^{-2}$
strain	ϵ	1
wedge half angle	ϕ	1
speed	V	LT^{-1}

Thus, this problem produces $7-3=4$ dimensionless quantities Π, shown as follows:

$$\Pi_1 = \epsilon, \quad \Pi_2 = \phi, \quad \Pi_3 = \frac{h}{b}, \quad \Pi_4 = E\rho^a V^b h^c, \tag{11}$$

where a, b, and c can be solved by dimensionless conditions;

$$\begin{aligned} \dim(\Pi_4) &= ML^{-1}T^{-2}M^aL^{-3a}L^bT^{-b}L^c \\ &= M^{1+a}L^{b-3a+c-1}T^{-2-b}, \end{aligned} \tag{12}$$

The following must be satisfied: $1+a=0$, $b-3a+c-1=0$, and $-2-b=0$. Thus, $a=-1$, $b=-2$, and $c=0$. The dimensionless quantities can be obtained by introducing the determined a, b and c into Π_4:

$$\Pi_4 = \frac{E}{\rho V^2}, \tag{13}$$

In this formula, E represents the elastic modulus, ρ represents the density, and V represents the speed at

which the rubber band springs back to the material point. Substituting $C = \sqrt{E/\rho}$ into the above equation to modify the dimensionless quantity Π_4, we obtain the following: $\Pi_4 = \frac{V}{C}$.

According to the theory of dimensional analysis, $\Pi_4 = f(\Pi_1, \Pi_2, \Pi_3)$, which can be written as follows:

$$\frac{V}{C} = f(\epsilon, \phi, \frac{h}{b}). \tag{14}$$

Thus, the ejection speed of the rubber band stretching is related to the strain ϵ, initial wedge half angle ϕ, and bending effect. The specific relationship must be determined by experiments.

References

1. Vermorel, R., Vandenberghe, N., Villermaux, E.: Rubber band recoil. Proc. R. Soc. A. 463,641-658(2007).https://doi.org/10.1098/rspa.2006.1781
2. Hickman, C.N.: The Dynamics of A Bow and Arrow. J. Appl. Phys. 8, 404–409(1937).https://doi.org/10.1063/1.1710314
3. Oratis, A.T., Bird, J.C.: Shooting Rubber Bands: Two Self-Similar Retractions for a Stretched Elastic Wedge. Phys. Rev. Lett. 122, 014102.1–014102.5(2019).https://doi.org/10.1103/PhysRevLett.122.014102
4. Gent, A.N., Marteny, P.: The effect of strain upon the velocity of sound and the velocity of free retraction for natural rubber. J. Appl. Phys. 53, 6069–6075(1982).https://doi.org/10.1063/1.331558
5. Stambaugh, R.B.: The Retraction of Stretched Rubber. Phys. Rev. Lett. 17, 617–618(1944).https://doi.org/10.1103/PhysRev.65.250
6. Audoly, B., Neukirch, S.: Fragmentation of Rods by Cascading Cracks: Why Spaghetti Does Not Break in Half. Phys. Rev. Lett. 95, 095505(2005).https://doi.org/10.1103/PhysRevLett.95.095505
7. Callan-Jones, A.C., Brun, P.T., Audoly, B.: Self-Similar Curling of a Naturally Curved Elastica. Phys. Rev. Lett. 108, 174302(2012).https://doi.org/10.1103/PhysRevLett.108.174302
8. Gladden, J.R., Handzy, N.Z., Belmonte, A., Villermaux, E.: Dynamic Buckling and Fragmentation in Brittle Rods. Phys. Rev. Lett. 94, 035503(2005).https://doi.org/10.1103/PhysRevLett.94.035503
9. Cross, R.C., Wheatland, M.S.: Modeling a falling slinky. Am. J. Phys. 80, 1051–1060(2012).https://doi.org/10.1119/1.4750489
10. Mason, P.: Finite Elastic Wave Propagation in Rubber. Proc. R. Soc. Lond. B. Biol. Sci. 272,315–330(1963).https://doi.org/10.2307/2414500
11. Wegner, J.L., Haddow, J.B., Tait, R.J.: Unloading Waves in a Plucked Hyperelastic String. J.Appl. Mech. 56, 459–465(1989).https://doi.org/10.1115/1.3176105
12. Wegner, J.L., Haddow, J.B.: An Experimental Study of the Unloading Waves in a Plucked Hyperelastic String. J. Appl. Mech. 57, 667–671(1990).https://doi.org/10.1115/1.2897074
13. Bauchau, O.A., Craig, J.I.: Euler-Bernoulli beam theory. solid mechanics and its applications 163, 173–221(2009)
14. Ballarini, R.: The Da vinci-Euler-Bernoulli beam theory. Mech. Eng.(2006)
15. Ömer, C., and Çiğdem, D.: The effect of strain upon the velocity of sound and the velocity of free retraction for natural rubber. Appl. Math. Model. 35, 2053–2067(2011)
16. Hassani, R., Ansari, R., Rouhi, H.: Large deformation analysis of 2D hyperelastic bodies based on the compressible nonlinear elasticity: A numerical variational method. Int. J. Non. Linear. Mech. 116, 39–54(2019).https://doi.org/10.1016/j.ijnonlinmec.2019.05.003
17. Michel, D., Giuseppe, S., Ivonne, S.: Methodical fitting for mathematical models of rubber like materials. P. Roy. Soc. A-Math. Phy. 473(2017).https://doi.org/10.1098/rspa.2016.0811
18. Upadhyay, K., Subhash, G., Spearot, D.: Thermodynamics-based stability criteria for constitutive equations of isotropic hyperelastic solids. J. Mech. Phys. Solids. 124, 115–142(2019).https://doi.org/10.1016/j.jmps.2018.09.038
19. Beda, T.: Modeling hyperelastic behavior of rubber: A novel invariant-based and a review of constitutive model. J. Polym. Sci. B. Polym. Phys. 45, 1713–1732(2007).https://doi.org/10.1002/polb.20928
20. Beda, T.: An approach for hyperelastic model-building and parameters estimation a review of constitutive models. Eur. Polym. J. 50, 97–108(2014).https://doi.org/10.1016/j.eurpolymj.2013.10.006
21. Gent, A.N.: A New Constitutive Relation for Rubber. Rubber. Chem. Technol. 69, 787–796(2012).https://doi.org/10.5254/1.3538357
22. Rivlin, R.S.: Large Elastic Deformations of Isotropic Materials. IV. Further Developments of the General Theory. Philos. T. R. Soc. A. 241, 379–397(1948).https://doi.org/10.1098/rsta.1948.0024
23. Mooney, M.: A Theory of Large Elastic Deformation. J. Appl. Phys. 11, 582–592(1940).https://doi.org/10.1063/1.1712836
24. Sun, B.H.: Dimensional Analysis and Lie Group.China High Education Press, in Chinese (2016).https://www.researchgate.net/publication/306396059_Dimensional_Analysis_and_Lie_Group

Figures

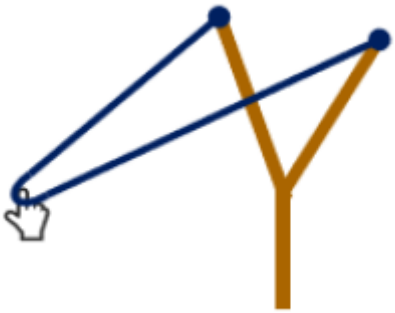

Figure 1

See the Manuscript Files section for the complete figure caption.

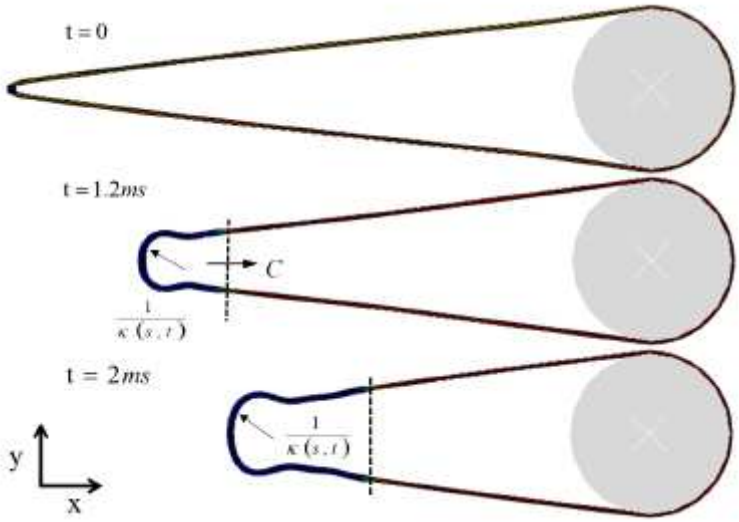

Figure 2

See the Manuscript Files section for the complete figure caption.

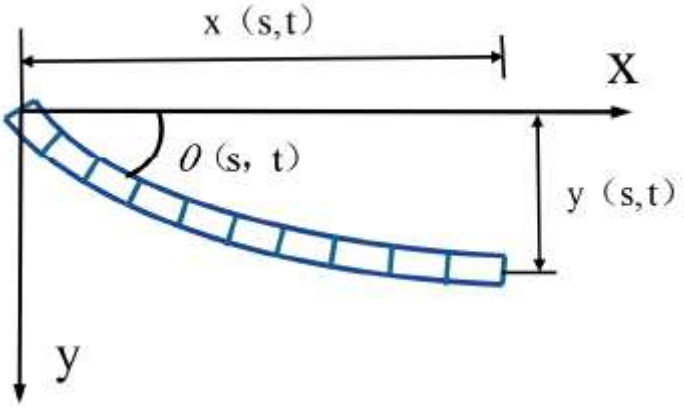

Figure 3

See the Manuscript Files section for the complete figure caption.

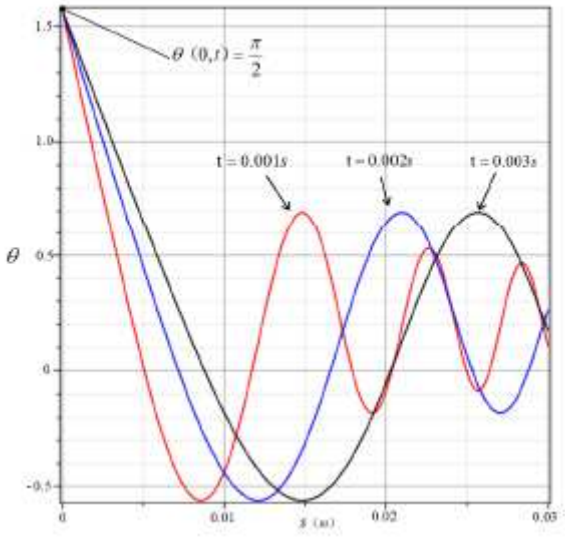

Figure 4

See the Manuscript Files section for the complete figure caption.

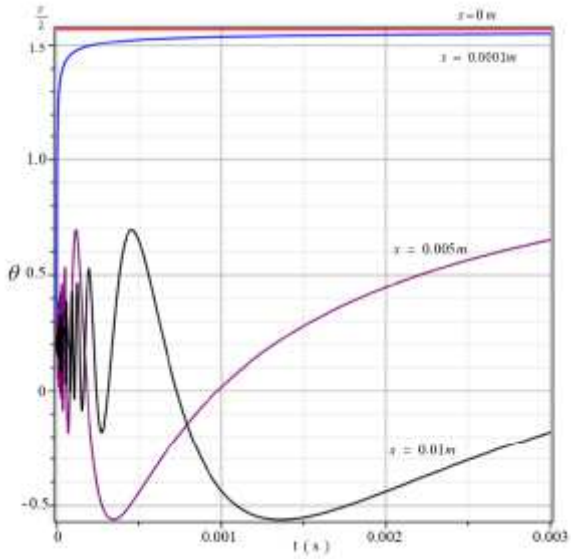

Figure 5

See the Manuscript Files section for the complete figure caption.

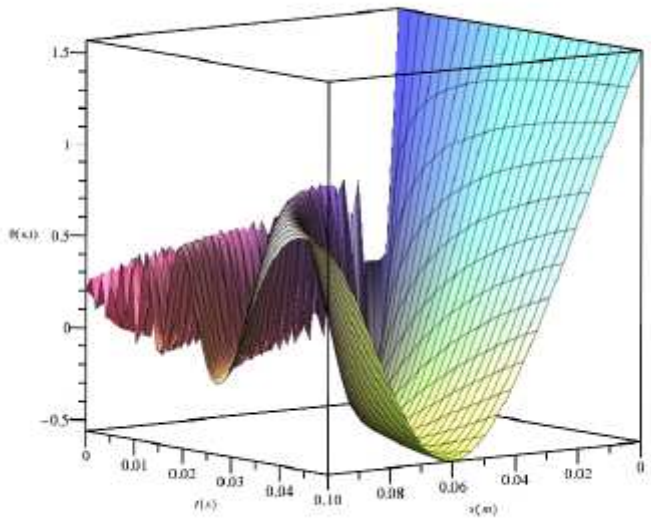

Figure 6

See the Manuscript Files section for the complete figure caption.

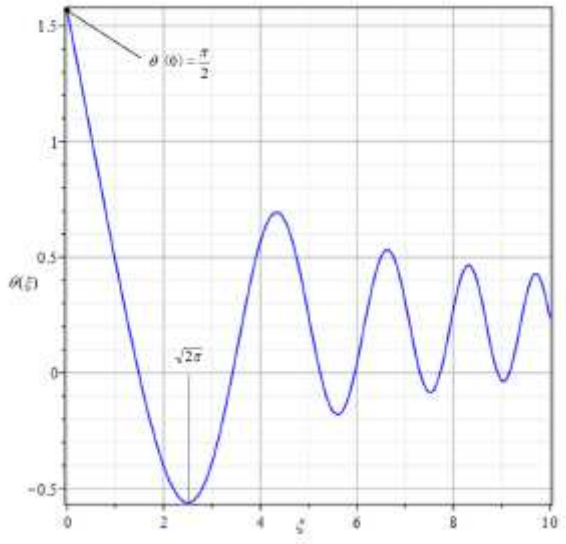

Figure 7

See the Manuscript Files section for the complete figure caption.

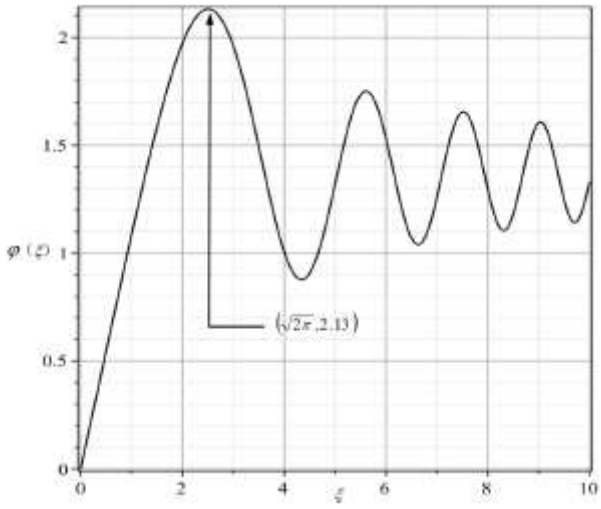

Figure 8

See the Manuscript Files section for the complete figure caption.

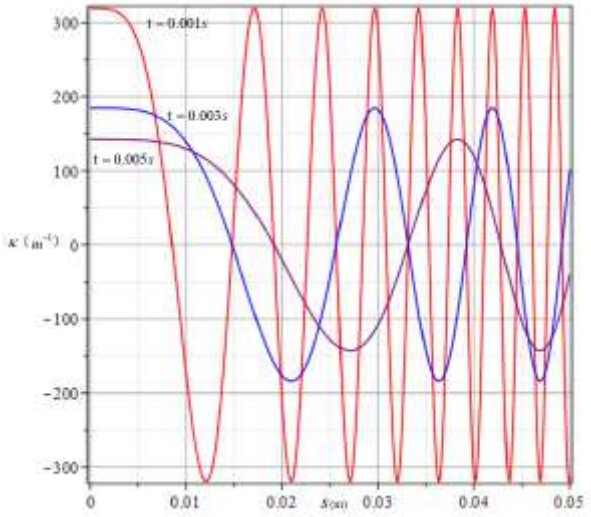

Figure 9

See the Manuscript Files section for the complete figure caption.

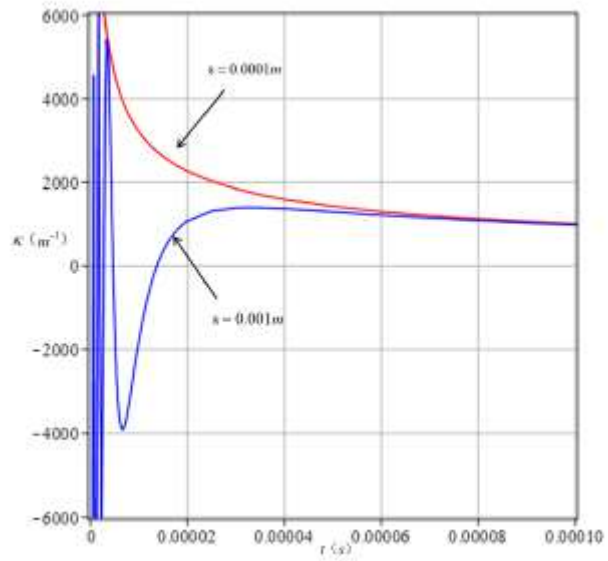

Figure 10

See the Manuscript Files section for the complete figure caption.

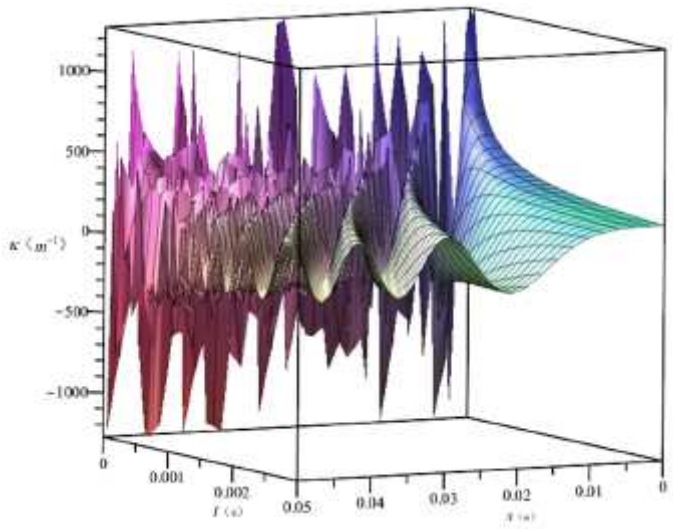

Figure 11

See the Manuscript Files section for the complete figure caption.

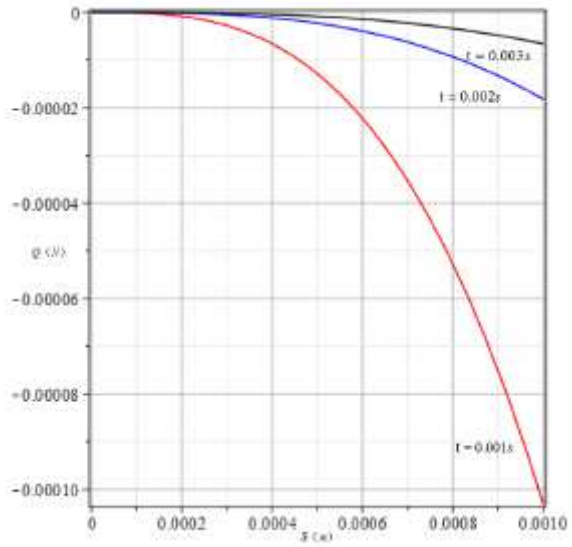

Figure 12

See the Manuscript Files section for the complete figure caption.

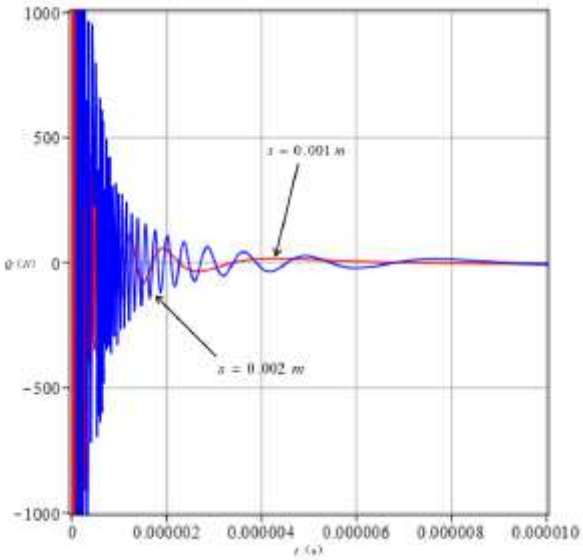

Figure 13

See the Manuscript Files section for the complete figure caption.

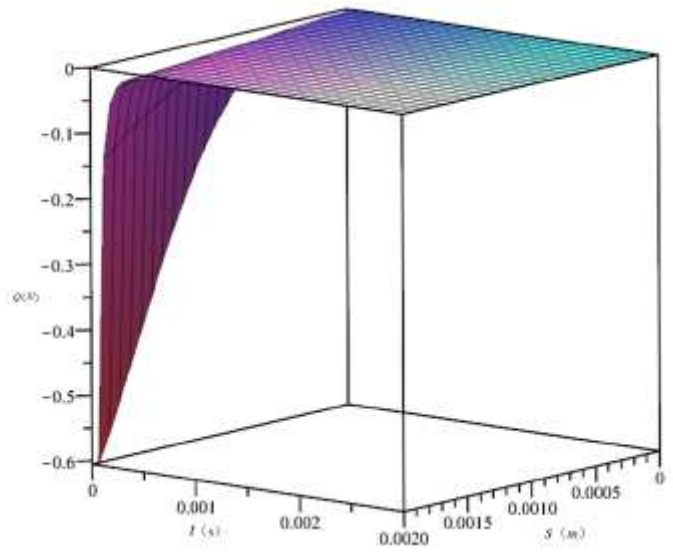

Figure 14

See the Manuscript Files section for the complete figure caption.

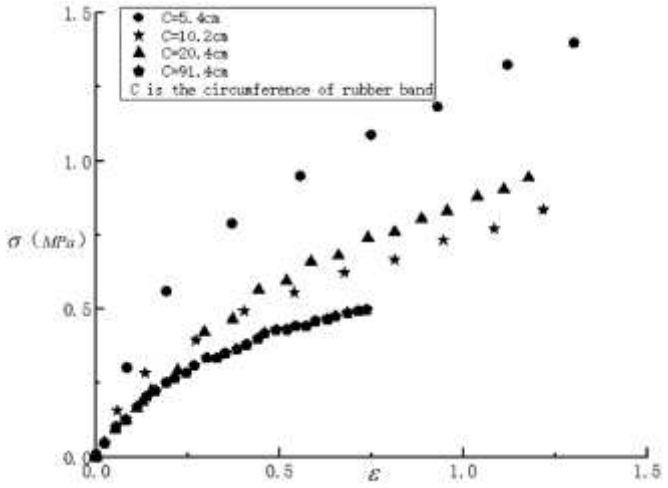

Figure 15

See the Manuscript Files section for the complete figure caption.

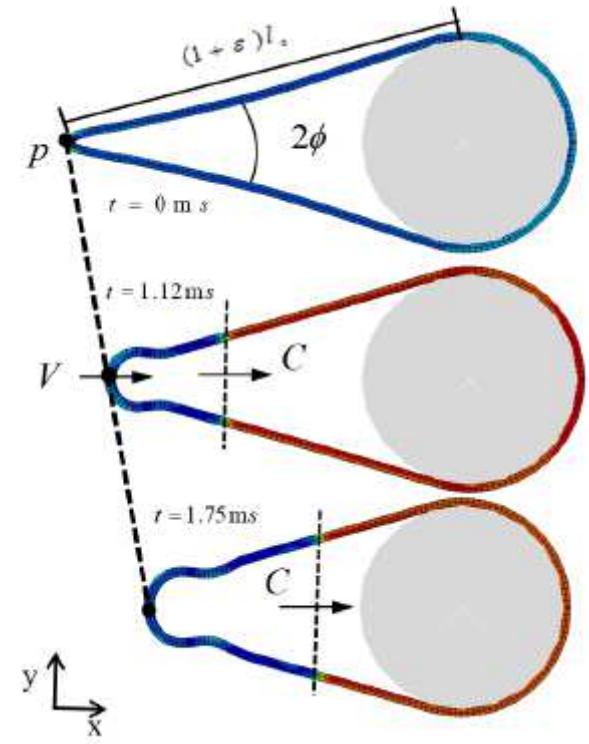

Figure 16

See the Manuscript Files section for the complete figure caption.

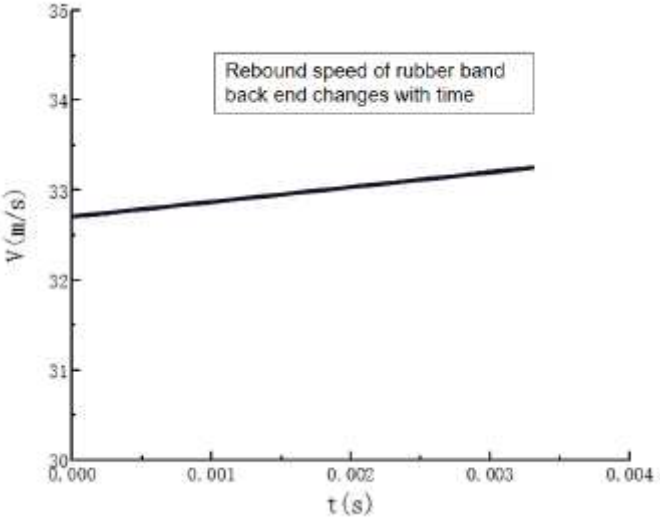

Figure 17

See the Manuscript Files section for the complete figure caption.

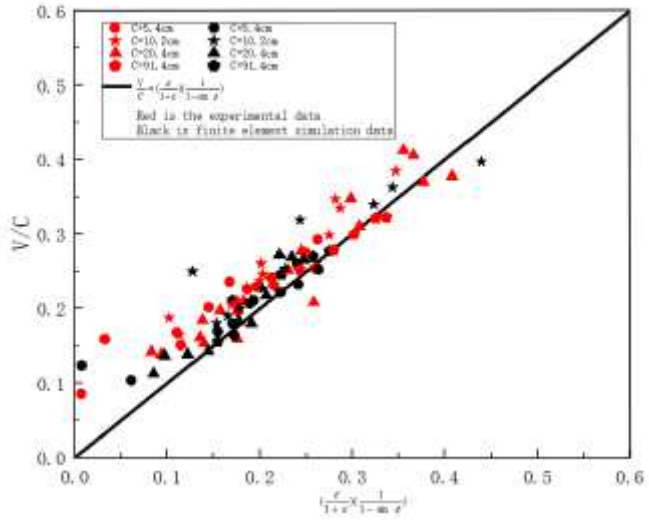

Figure 18

See the Manuscript Files section for the complete figure caption.

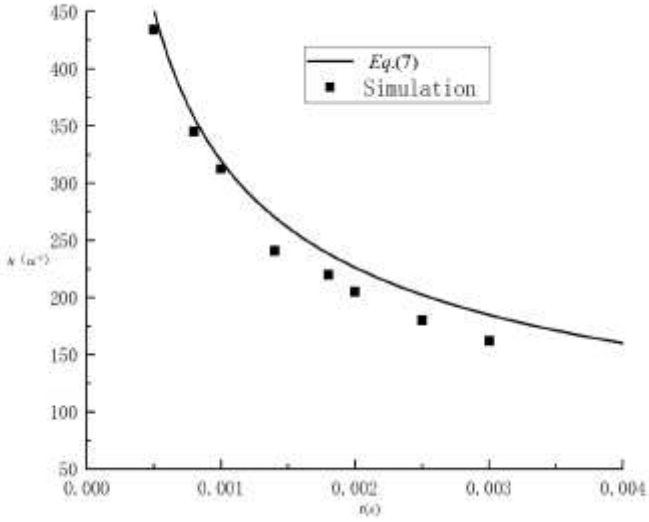

Figure 19

See the Manuscript Files section for the complete figure caption.

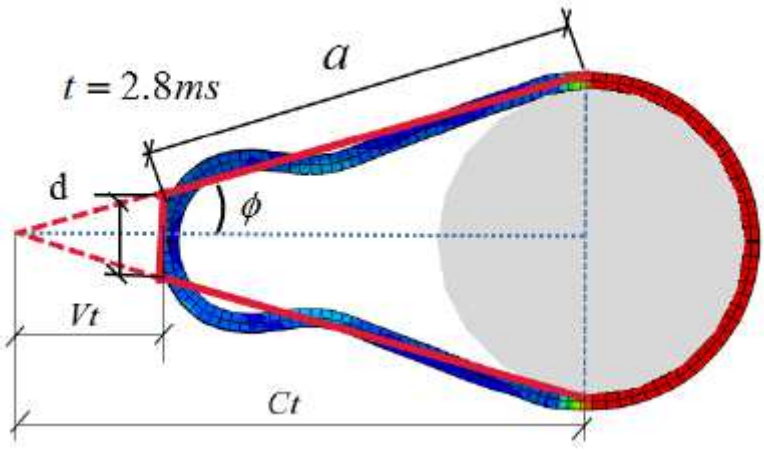

Figure 20

See the Manuscript Files section for the complete figure caption.

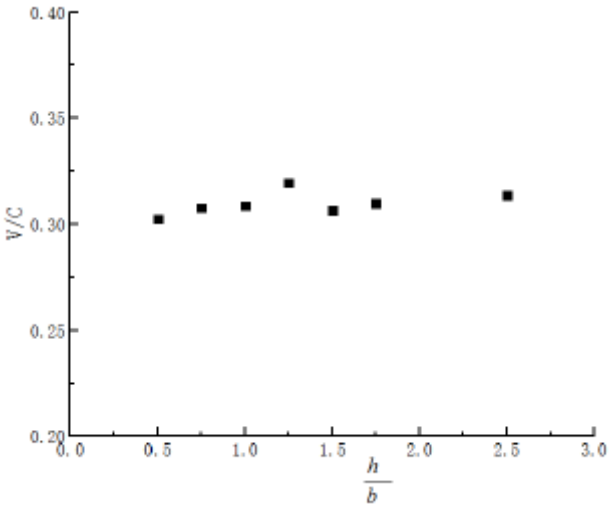

Figure 21

See the Manuscript Files section for the complete figure caption.

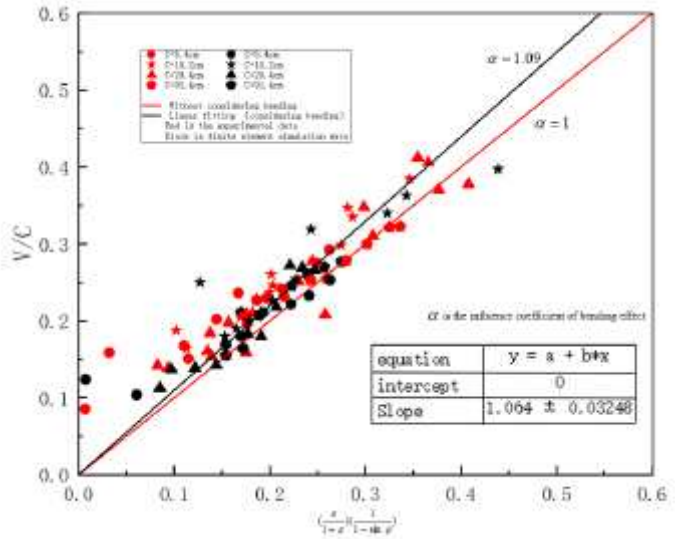

Figure 22

See the Manuscript Files section for the complete figure caption.

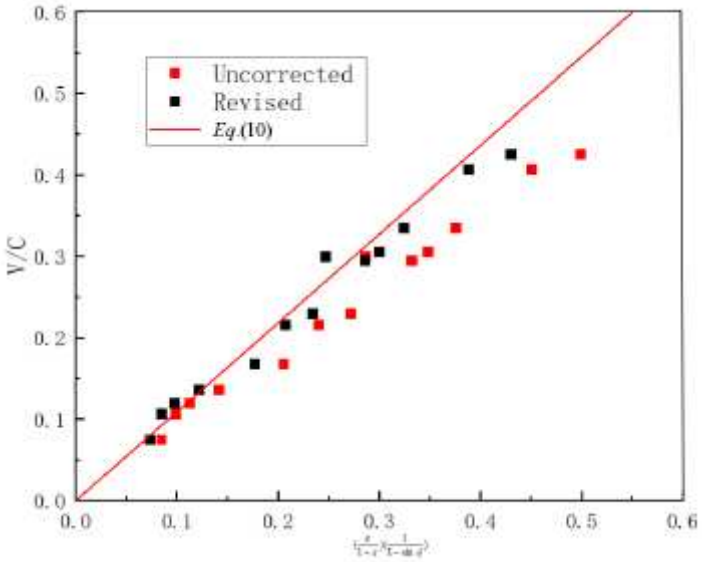

Figure 23

See the Manuscript Files section for the complete figure caption.

Supplementary Files

This is a list of supplementary files associated with this preprint. Click to download.

- video.mp4